Design of a 3D CNT/$Ti_3C_2T_x$ aerogel-modified separator for Li–S batteries to eliminate both the shuttle effect and slow redox kinetics of polysulfides

YIN Fei, JIN Qi, ZHANG Xi-tian*, WU Li-li*

(*Key Laboratory for Photonic and Electronic Bandgap Materials*, *Ministry of Education*, *School of Physics and Electronic Engineering*, *Harbin Normal University*, *Harbin* 150025, *China*)

Abstract: Lithium–sulfur (Li–S) batteries suffer from fast capacity fade and an inferior rate performance due to the shuttling of polysulfides (LiPSs) and slow redox kinetics. To solve these issues, a three-dimensional (3D) CNT/$Ti_3C_2T_x$ aerogel was prepared, with $Ti_3C_2T_x$ as the active matrix and CNTs as the conductive pillars, and used as a LiPS immobilizer and promoter to modify a commercial Li–S battery separator. The unique design of highly porous 3D aerogel results in the exposure of more $Ti_3C_2T_x$ active sites by preventing the restacking of their sheets, which not only provides abundant charge transport paths, but also strengthens the adsorption and catalytic conversion of LiPSs. The incorporation of CNTs forms a highly conductive network to connect the adjacent $Ti_3C_2T_x$ sheets, thereby improving the conductivity and robustness of the 3D aerogel. As a result, a Li–S cell using the CNT/ $Ti_3C_2T_x$ aerogel-modified separator has a high rate capacity of 1 043.2 mAh g^{-1} up to 2 C and an excellent cycling life of over 800 cycles at 0.5 C with a low capacity decay rate of 0.07% per cycle.

Key words: CNTs; $Ti_3C_2T_x$; Aerogel; Separator; Lithium-sulfur batteries

1 Introduction

Lithium–sulfur (Li–S) batteries have become the most promising next-generation rechargeable energy storage devices because of their high theoretical energy density (2 600 Wh kg^{-1}), low cost and non-toxicity. However, several inherent shortcomings obstruct their commercial development[1–2]. First, poor electronic conductivity of S and its final discharge products Li_2S_2/Li_2S causes large electrochemical polarization and low active material utilization rate. Second, severe shuttle effect of soluble polysulfides (LiPSs) leads to low Coulomb efficiency and rapid capacity decay. Third, sluggish redox kinetics results in inferior rate performance. Although the above drawbacks have been significantly improved by the reasonable design of S cathode[3–4], electrolyte[5–6] and anode[7–8], soluble LiPSs still inevitably escape from the cathode surface and diffuse to the anode through the highly porous separator, resulting in poor cycle life and serious anode corrosion.

Modifying commercial separators for Li–S batteries with functional materials is a simple and effective approach to prevent the diffusion of LiPSs[9–10]. Initially, carbon materials are usually employed to modify separators of Li–S batteries, which could physically adsorb LiPSs and be served as the second collector to increase the conductivity on the cathode side[11–13]. However, the weak affinity of LiPSs with these non-polar carbon materials leads to severe capacity degradation during long-term cycling. For this reason, various polar adsorbents, including metal-organic frameworks, metal oxides and sulfides, have been developed to chemically adsorb LiPSs[14–17]. Unfortunately, only through the single chemisorption mechanism, too much adsorbed LiPSs will accumulate on the surface of the separator, resulting in limited ion diffusion and slow reaction kinetics. Catalyzing the conversion of adsorbed LiPSs could shorten the residence time of soluble intermediates in the electrolyte, thereby effectively alleviating the LiPS shuttle. Based on the above analysis, the ideal separat-

Received date: 2021-05-13; **Revised date:** 2021-07-03

Corresponding author: ZHANG Xi-tian, Ph.D, Professor. E-mail: xtzhangzhang@hotmail.com;
WU Li-li, Ph.D, Professor. E-mail: wll790107@hotmail.com

Author introduction: YIN Fei, Master Student. E-mail: 761578835@qq.com

or modified material should own the following advantages: (1) fast ion/electron conduction to ensure high S utilization rate, (2) strong LiPS affinity to effectively suppress their diffusion and (3) high catalytic activity to accelerate the conversion of adsorbed LiPSs.

Recently, numerous researches demonstrate that incorporating two-dimensional (2D) MXene materials into the Li–S battery system can promote the rate capability and cycling life of Li–S batteries. Among them, $Ti_3C_2T_x$ is widely studied due to its abundant surface groups and excellent electronic conductivity[18–22]. The surface groups (mainly —OH groups) and Ti sites of $Ti_3C_2T_x$ can effectively capture the LiPSs through the thiosulfate/polythionate disproportionation mechanism and Lewis acid-base interaction so as to alleviate the LiPS shuttle. Besides that, the highly conductive Ti—C—Ti core endows $Ti_3C_2T_x$ with high catalytic activity, which can offer fast charge transfer to accelerate the liquid-solid conversion between LiPSs and Li_2S, thereby improving the redox kinetics[23–24]. Based on the synergistic advantages of LiPS adsorption and catalytic conversion, $Ti_3C_2T_x$ is believed to be a promising material to modify the polypropylene（PP）separator. However, the severe restacking phenomenon caused by Vander Waals interactions often hinders the rapid migration of ions and the full utilization of $Ti_3C_2T_x$ active sites.

Construction of three-dimensional (3D) porous structure is regarded as a desirable strategy to overcome this issue[25–26], which can not only effectively avoid the $Ti_3C_2T_x$ restacking to reduce the ion diffusion barrier, but also help to fully expose the active sites of $Ti_3C_2T_x$, thereby improving its ability to adsorb and catalytically convert LiPSs. Our group previously coated a 3D $Ti_3C_2T_x$ aerogel on the PP separator for Li–S batteries, achieving excellent electrochemical performance[27]. However, the poor mechanical strength makes it difficult for the $Ti_3C_2T_x$ aerogel to maintain a robust porous structure during the long-term cycle. According to previous report[28], CNTs can act as effective supporting-pillars bridging $Ti_3C_2T_x$ sheets to enhance the mechanical stability of the 3D porous structure. At the same time, incorporating conductive CNTs into the $Ti_3C_2T_x$ matrix benefits to establish a connected conductive network at the separator/cathode interface, thereby greatly improving the conductivity of the composed aerogel. Inspired by this, it is reasonable to combine the advantages of $Ti_3C_2T_x$ and CNTs network to fabricate a highly active, robust and conductive aerogel skeleton as the ideal separator modification material.

Herein, a 3D CNT/$Ti_3C_2T_x$ aerogel with excellent electronic conductivity, strong adsorption ability and high catalytic activity was developed, and used as the separator modifier for Li–S batteries. As expected, the obtained CNT/$Ti_3C_2T_x$ aerogel modified separator obviously restrains the LiPS shuttle and accelerates the LiPS conversion kinetics. Therefore, Li–S cells assembled with the CNT/$Ti_3C_2T_x$ aerogel modified separator show significantly enhanced rate capability and stable cycle performance.

2 Experimental

2.1 Preparation of KB/S electrode

The mixture of Ketjen Black (KB) powder and S powder was ground for 30 min, and then heated at 155 °C overnight to synthesize KB/S composite material with a S content of 70%.

To prepare the KB/S electrode, 70% of KB/S composite, 20% of acetylene black, 10% of poly(1,1-difluoroethylene) (PVDF) binder and an appropriate amount of N-methylpyrrolidone (NMP) solution were mixed, and then coated on the Al foil. The coated Al foil was vacuum-dried at 60 °C, and then cut into 13 mm.

2.2 Preparation of the modified separator

The synthesis process of CNT/$Ti_3C_2T_x$ aerogel is as follows. First, a mixture of ethylenediamine solution (100 μL), CNT aqueous dispersion (0.5 mL, 40 mg mL^{-1}) and $Ti_3C_2T_x$ solution (4 mL, 20 mg mL^{-1}) was ultrasonically dispersed for 10 min. Then, the mixed solution was sealed in a reagent bottle and heated at 140 °C for 6 h to form a hydrogel. To remove the remaining impurities, this hydrogel was

washed repeatedly with deionized (DI) water. Finally, the washed hydrogel was freeze-dried for 24 h to obtain the CNT/$Ti_3C_2T_x$ aerogel. As a comparison, the concentrated $Ti_3C_2T_x$ solution was directly freeze-dried to prepare $Ti_3C_2T_x$ powder.

The CNT/$Ti_3C_2T_x$ aerogel and PVDF binder were added in NMP at a mass ratio of 9∶1 and ultrasonically dispersed for 20 min to form a uniform dispersion. Then it was vacuum filtered onto a Celgard 2400 PP separator to obtain a CNT/$Ti_3C_2T_x$ aerogel modified separator. The separator was punched into 19 mm. The mass loading of the CNT/$Ti_3C_2T_x$ aerogel on the PP separator is about 0.8 mg cm^{-2}. As a comparison, we also prepared the $Ti_3C_2T_x$ modified separator using the $Ti_3C_2T_x$ powder in the same way.

2.3 LiPS adsorption experiment

First, Li_2S and S (molar ratio: 1∶5) were put into 1,2-dimethoxyethane (DME)/1,3-dioxolane (DOL) (1∶1, *v*/*v*) solution. This mixture was stirred overnight at 60 °C in a glovebox to obtain a Li_2S_6 solution (0.01 mol L^{-1}). Then, the CNT/$Ti_3C_2T_x$ aerogel and $Ti_3C_2T_x$ powder were immersed in 1 mL of the Li_2S_6 solution for adsorption experiments.

2.4 Symmetrical cell test

In order to prepare symmetric cell electrodes, CNT/$Ti_3C_2T_x$ aerogel (or $Ti_3C_2T_x$) and PVDF binder (mass radio: 9∶1) were mixed with NMP, and then coated on a carbon paper. After drying, the coated carbon paper was cut into 13 mm disks. The mass loading of the CNT/$Ti_3C_2T_x$ aerogel (or $Ti_3C_2T_x$) in each disk is approximately 1 mg cm^{-2}. To assemble the symmetric cell, we used the CNT/$Ti_3C_2T_x$ aerogel (or $Ti_3C_2T_x$) electrode as a working/counter electrode, the PP separator as a separator, 20.0 μL of DOL/DME (1∶1, *v*/*v*) solution containing 1 mol L^{-1} LiTFSI as blank electrolyte, and 20.0 μL of Li_2S_6 solution (0.1 mol L^{-1}) as catholyte. Cyclic voltammetry (CV) test of the symmetrical cell was performed on the VMP3 electrochemical workstation with a voltage window of −0.8-0.8 V and a scan rate of 50 mV s^{-1}.

2.5 Li_2S nucleation deposition

The CNT/$Ti_3C_2T_x$ aerogel (or $Ti_3C_2T_x$) was dispersed in ethanol and then coated onto a carbon paper (diameter: 13 mm) to make electrodes. The cell was assembled by using the CNT/$Ti_3C_2T_x$ aerogel (or $Ti_3C_2T_x$) electrode, PP separator and Li foil as the working electrode, separator, and counter electrode, respectively. The catholyte was Li_2S_8/TEGDME solution (0.25 mol L^{-1}) containing 1 mol L^{-1} LiTFSI. We dropped Li_2S_8 catholyte (20 μL) into the CNT/$Ti_3C_2T_x$ aerogel (or $Ti_3C_2T_x$) working electrode, and added blank electrolyte (20 μL) containing 2% $LiNO_3$ into the counter electrode. On the VMP3 multi-channel electrochemical workstation, the cell was discharged to 2.06 V by a constant current (0.112 mA), and subsequently kept at a constant potential of 2.05 V.

2.6 Material characterization and electrochemical testing

A scanning electron microscope (SEM; SU70, Hitachi, Japan), a transmission electron microscope (TEM) and an X-ray diffractometer (Rigaku D/max2600) were employed to investigate the morphologies and to characterize the microstructures of the CNT/$Ti_3C_2T_x$ aerogel and $Ti_3C_2T_x$. The ASAP 2010 analyzer was used to measure nitrogen absorption/desorption isotherms. To measure the CNT content, thermogravimetric analysis (TG, Diamond 6300) was conducted in air from room temperature to 900 °C.

CR2025 cell was assembled with Li foil as the anode, the CNT/$Ti_3C_2T_x$ modified aerogel separator, $Ti_3C_2T_x$ modified separator or PP separator as the separator, KB/S electrode as the cathode, DME/DOL (1∶1, *v*/*v*) solution containing 2% $LiNO_3$ and 1 mol L^{-1} LiTFSI as the electrolyte. The S loading of each cathode is about 1 mg cm^{-2}. The electrolyte/S ratio is approximately 15 μL mg^{-1}, so the electrolyte amount of each cell is about 20 μL. Electrochemical impedance spectra (EIS) and CV curves were measured on a VMP3 multi-channel workstation (BioLogic, France). The frequency range of EIS measurement is 10 mHz to 100 kHz. The scan rate and voltage window of the CV test are 0.1 mV s^{-1} and 1.7-2.8 V, respectively. LANCT battery test system was used to perform the galvanostatic charge-discharge (GCD) test with a voltage range of 1.7-2.8 V.

2.7 The calculation method of the CNT content

At 900 °C in air, the $Ti_3C_2T_x$ in the aerogel will be completely converted into TiO_2[29], and the CNTs in the aerogel will be lost due to the combustion reaction[30]. After the TG test, the mass fraction of pure $Ti_3C_2T_x$ changed from 100% to 105.2%, while the mass fraction of CNT/$Ti_3C_2T_x$ aerogel changed from 100% to 77.5%. The content of $Ti_3C_2T_x$ in CNT/$Ti_3C_2T_x$ aerogel can be calculated by the following equation:

$$\frac{100.0\%}{105.2\%} = \frac{x}{77.5\%}, \quad x = 73.7\%.$$

Therefore, the content of CNTs in CNT/$Ti_3C_2T_x$ aerogel is about 26.3%.

3 Results and discussion

3.1 Morphology and structure

Fig. 1a is the SEM image of the pristine $Ti_3C_2T_x$, which exhibits a 2D lamellar morphology with the lateral size of several micrometers. In contrast, CNT/$Ti_3C_2T_x$ aerogel shows a 3D porous network structure composed of wrinkled $Ti_3C_2T_x$ sheets and net-like CNTs (Figs. 1b and c). According to N_2 adsorption/desorption isotherms (Fig. 1d), the specific surface area of CNT/$Ti_3C_2T_x$ aerogel is 3.5 times that of $Ti_3C_2T_x$, implying the effective suppression of $Ti_3C_2T_x$ restacking, which is helpful to offer more active sites to chemically trap soluble LiPSs[27]. In addition, the larger pore volume of CNT/$Ti_3C_2T_x$ aerogel (Fig. 1e) also contributes to physically encapsulate LiPSs and ensure fast ion transport as well as smooth electrolyte infiltration, leading to the increased active material utilization. Hall tests were conducted to measure the electrical conductivity of the two samples. As shown in Fig. 1f, the electrical conductivity of the CNT/$Ti_3C_2T_x$ aerogel modified separator (2.51 S cm^{-1}) is higher than that of the $Ti_3C_2T_x$ modified separator (1.18 S cm^{-1}), proving that the incorporation of CNTs plays an important role in facilitating electron transfer.

Fig. 2a and its inset are the TEM images of different areas of the CNT/$Ti_3C_2T_x$ aerogel, showing that the surface of $Ti_3C_2T_x$ is decorated with hollow CNTs, but what is unsatisfactory is that the CNTs are not uniformly distributed. The high-resolution TEM (HRTEM) images of the CNT/$Ti_3C_2T_x$ aerogel in Figs. 2b and 2c further confirm the successful combination of CNTs and $Ti_3C_2T_x$, in which the lattice fringe spacing of 0.22 nm corresponds to the (104) plane of $Ti_3C_2T_x$. Energy dispersive X-ray (EDX) spec trum and elemental mapping images in Figs. 2d and 2e show the characteristic elements Ti, C, O and Cl of $Ti_3C_2T_x$. At

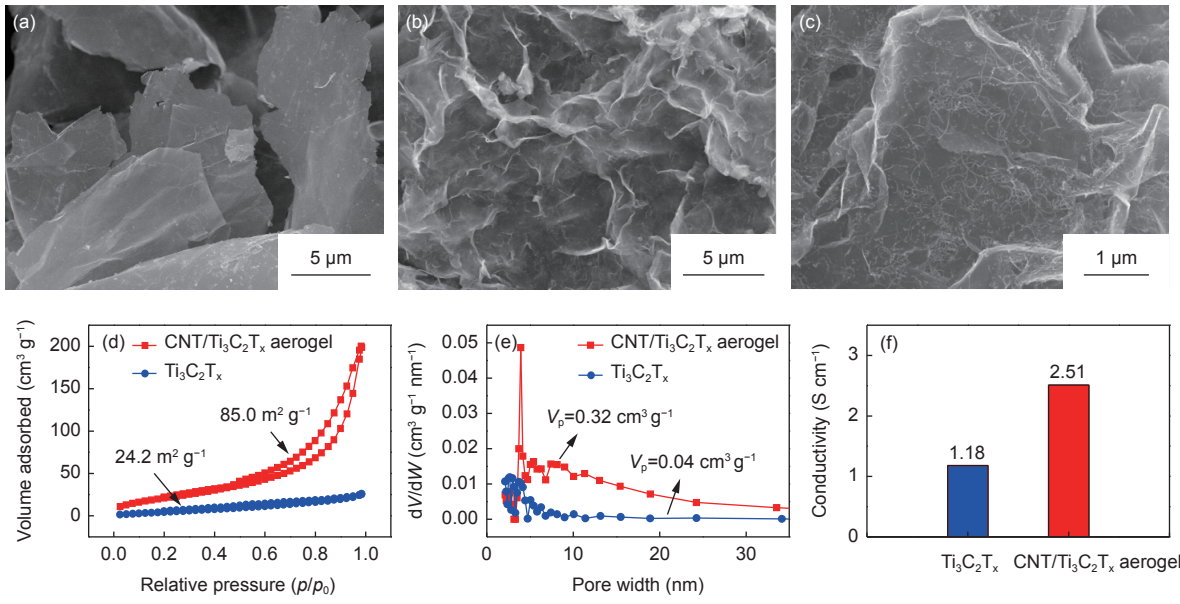

Fig. 1 SEM images of (a) $Ti_3C_2T_x$ and (b, c) CNT/$Ti_3C_2T_x$ aerogel. (d) N_2 adsorption-desorption isotherms. (e) Pore size distributions. (f) Electrical conductivities of the $Ti_3C_2T_x$ modified separator and CNT/$Ti_3C_2T_x$ aerogel modified separator.

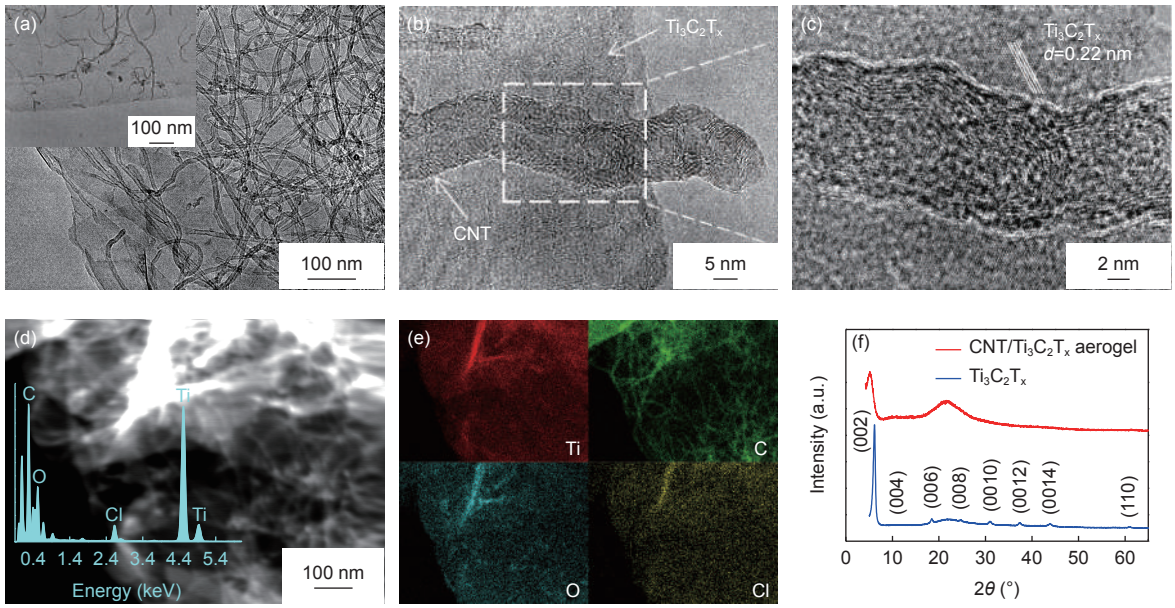

Fig. 2 (a) TEM images of different areas of the CNT/$Ti_3C_2T_x$ aerogel. (b, c) HRTEM images of the CNT/$Ti_3C_2T_x$ aerogel. (d, e) EDX spectrum and elemental mappings of the CNT/$Ti_3C_2T_x$ aerogel. (f) XRD patterns.

the same time, the outline of CNTs can be clearly seen in the C element mapping. XRD analysis was used to further compare the crystal structure characteristics of the CNT/$Ti_3C_2T_x$ aerogel and $Ti_3C_2T_x$. The XRD pattern of CNT/$Ti_3C_2T_x$ aerogel in Fig. 2f shows the typical $Ti_3C_2T_x$ diffraction peak[27] and the characteristic peak of carbon materials (~ 24°), suggesting the successful introduction of CNTs into the $Ti_3C_2T_x$ matrix. Different from the pristine $Ti_3C_2T_x$, the (002) peak of $Ti_3C_2T_x$ in the CNT/$Ti_3C_2T_x$ aerogel shifts to the left, illustrating the increased interlayer *d*-spacing by the design of 3D aerogel structure.

To optimize the proportion of CNTs in the aerogel, the cycle performance of the cells with CNT/$Ti_3C_2T_x$ aerogel modified separators with different CNT contents (10%, 20% and 30%) at 0.5 C were evaluated in Fig. 3a. By comparison, the cell with the CNT/$Ti_3C_2T_x$ aerogel modified separator with 20% CNTs shows the best cycle stability, while the cycle performance of that with 10% CNTs is slightly worse, because the low content of CNTs cannot offer the sufficient conductivity to ensure fast electron transfer. When the content of CNTs increases to 30%, too much CNTs will weaken the adsorption and catalytic effects of $Ti_3C_2T_x$ to LiPSs, resulting in rapid capacity decay. Therefore, the following measurements

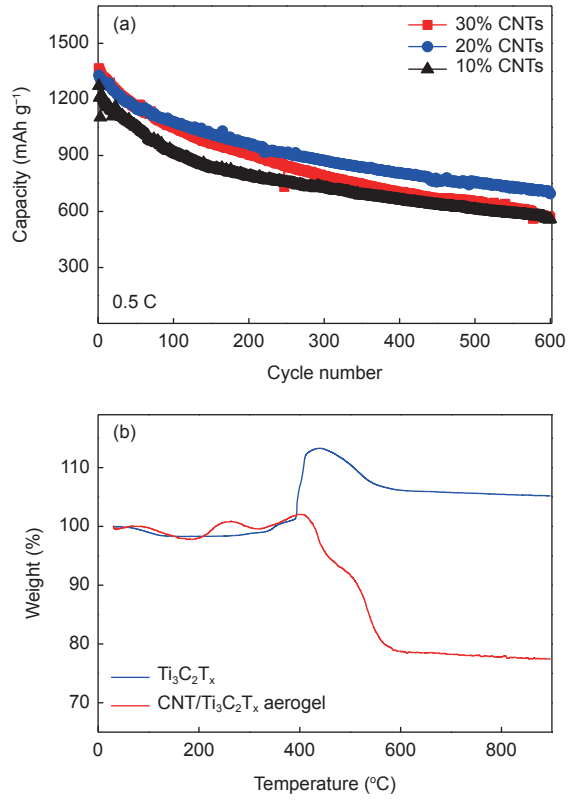

Fig. 3 (a) Cycling performance of the cells with CNT/$Ti_3C_2T_x$ aerogel modified separators with different CNT contents. (b) TG curves of $Ti_3C_2T_x$ and the CNT/$Ti_3C_2T_x$ aerogel.

were based on the CNT/$Ti_3C_2T_x$ aerogel with 20% CNTs. It is worth noting that we define the CNT content as 20% based on the mass ratio (8 ∶ 2) of $Ti_3C_2T_x$ and CNTs added during the preparation process.

While the actual content of CNTs calculated by thermogravimetric (TG) analysis is about 26.3% (Fig. 3b). This inconsistency may be caused by the uneven distribution of CNTs in the aerogel.

3.2 The effect of CNT/$Ti_3C_2T_x$ aerogel on LiPSs

Effective LiPS adsorption ability is an important factor for separator modification materials to mitigate the shuttle effect. Visual adsorption experiments were carried out to compare the LiPS adsorption ability of the CNT/$Ti_3C_2T_x$ aerogel and $Ti_3C_2T_x$ by immersing them in 0.01 mol L^{-1} Li_2S_6 solution for 6 h. As shown in Fig. 4a, the Li_2S_6 solution impregnated with the CNT/$Ti_3C_2T_x$ aerogel becomes almost colorless, while the solution with $Ti_3C_2T_x$ is still light yellow, indicating the enhanced LiPS adsorption capacity of the CNT/$Ti_3C_2T_x$ aerogel.

High electrocatalytic activity is another key factor to ensure effective LiPS confinement by promoting their conversion. To further compare the catalytic ability of the CNT/$Ti_3C_2T_x$ aerogel and $Ti_3C_2T_x$ towards LiPSs, we conducted CV tests of symmetrical cells (Fig. 4b). Clearly, the current density of the CNT/$Ti_3C_2T_x$ aerogel electrode is about three times that of the $Ti_3C_2T_x$ electrode, indicating the higher activity of CNT/$Ti_3C_2T_x$ aerogel to catalyze liquid-phase LiPSs conversion, which is beneficial to ensure fast ion transfer by minimizing the accumulation of adsorbed LiPSs on the separator surface. Besides that, evaluating the deposition behavior of solid Li_2S on the substrate is also necessary to study the conversion reaction kinetics[23]. Here, we conducted Li_2S nucleation deposition experiments by using Li foil as the anode, $Ti_3C_2T_x$ electrode or CNT/$Ti_3C_2T_x$ aerogel electrode as the cathode, and Li_2S_8/TEGDME solution as the catholyte. As shown in Figs. 4c and 4d, the precipitation capacities of Li_2S on $Ti_3C_2T_x$ and the CNT/$Ti_3C_2T_x$ aerogel are 189.1 and 232.6 mAh g^{-1}, respectively, indicating the better catalytic effect of the CNT/$Ti_3C_2T_x$ aerogel to induce effective nucleation and deposition of Li_2S. As discussed above, the CNT/$Ti_3C_2T_x$ aerogel with high conductivity and abundant active sites can serve as an effective catalyst to promote the reaction kinetics of liquid LiPS conversion and solid Li_2S deposition, thereby reducing the LiPS diffusion and improving the utilization rate of S.

3.3 Electrochemical performance of batteries

To verify the effectiveness of the CNT/$Ti_3C_2T_x$ aerogel modified separator in improving the rate capability and cycling life of Li–S batteries, the PP separator, $Ti_3C_2T_x$ modified separator and CNT/$Ti_3C_2T_x$ aerogel modified separator were assembled in

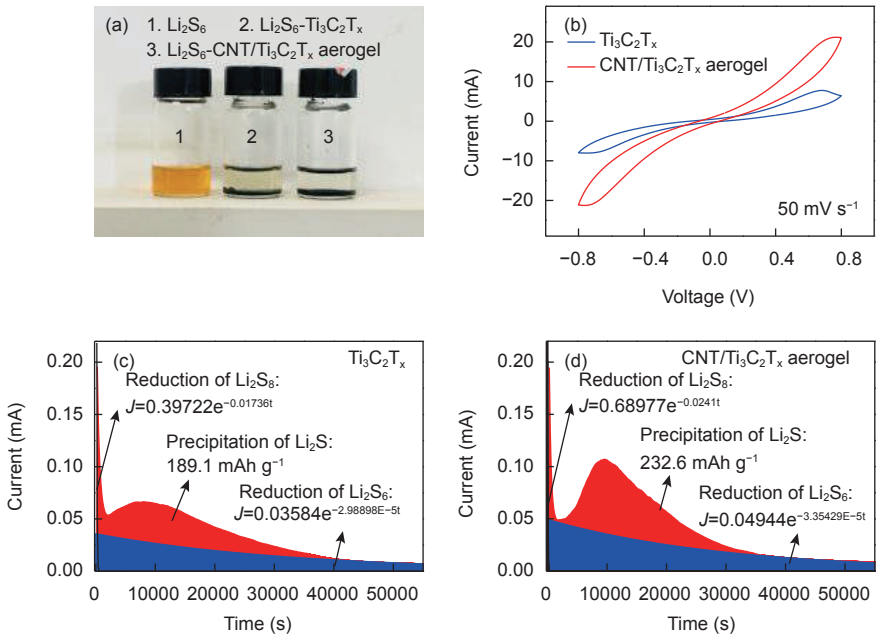

Fig. 4　(a) Digital images of Li_2S_6 solution after contacting with $Ti_3C_2T_x$ or CNT/$Ti_3C_2T_x$ aerogel for 6 h. (b) CV curves of the $Ti_3C_2T_x$ and CNT/$Ti_3C_2T_x$ aerogel symmetric cells. Potentiostatic discharge of the Li_2S_8/TEGDME catholyte on (c) $Ti_3C_2T_x$ and (d) the CNT/$Ti_3C_2T_x$ aerogel electrodes at 2.05 V.

CR2025 cells with KB/S as the cathode. They are named KB/S, KB/S-T and KB/S-CT cells respectively. Fig. 5a shows the CV curves of these cells at 0.1 mV s^{-1}. All curves exhibit two typical reduction peaks, a and b, corresponding to the solid-liquid-solid conversion from elemental S to soluble LiPSs and then to insoluble Li_2S, respectively. Meanwhile, an obvious oxidation peak c also can be observed, corresponding to the reversible conversion from Li_2S to LiPSs and finally to S. By comparison, the CV curve of the KB/S-CT cell has the largest positive shift on the cathodic peak and the largest negative shift on the anodic peak, indicating the lowest electrochemical polarization. Furthermore, all the CV peaks of the KB/S-CT cell are the sharpest, suggesting that the utilization of active materials is increased due to effective LiPS adsorption and enhanced redox kinetics. Next, EIS curves of KB/S, KB/S-T and KB/S-CT cells were further measured to reveal the charge transfer kinetics, as shown in Fig. 5b. All curves exhibit a semicircle in the high-frequency region and a diagonal line in the low-frequency region, corresponding to the charge transfer resistance (R_{ct}) and lithium-ion diffusion resistance (Z_w), respectively. In addition, the high-frequency intercept on the real axis relates to the ionic resistance of the electrolyte (R_s)[31]. In order to provide more precise impedance values, we fit the EIS data based on the equivalent circuit in inset of Fig. 5b, and the corresponding fitting results are shown in Fig. 5c. Clearly, the KB/S-CT cell shows the lowest R_s and R_{ct},

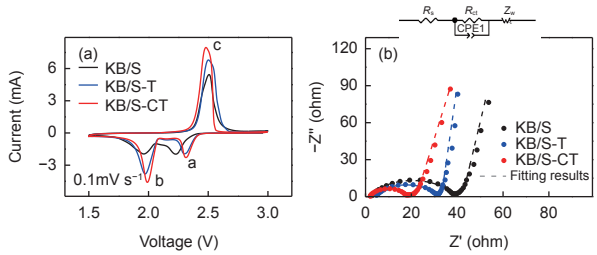

(c)	KB/S	KB/S-T	KB/S-CT
R_s (Ω)	2.5	4.4	2.0
R_{ct} (Ω)	35.1	26.1	15.5

Fig. 5 (a) CV curves of the KB/S, KB/S-T and KB/S-CT cells. (b) EIS curves of the KB/S, KB/S-T and KB/S-CT cells. (Inset is the equivalent circuit for EIS fitting). (c) EIS fitting results.

indicating its excellent electron transfer capability. While, the KB/S-T cell assembled with the $Ti_3C_2T_x$ modified separator exhibits the highest R_s value. This can be attributed to the unsmooth electrolyte infiltration caused by $Ti_3C_2T_x$ restacking phenomenon. Therefore, the CNT/$Ti_3C_2T_x$ aerogel modified separator can not only be used as a LiPS reservoir to effectively inhibit the LiPS shuttle, but also as a second current collector to enhance the cathode conductivity.

Generally, at low current density, the longer charge-discharge time will prolong the diffusion time of LiPSs, leading to a more serious shuttle effect. Therefore, it is of great significance to study the cycle performance of the cell at low current density. Fig. 6a shows the cycle performance of the KB/S, KB/S-T and KB/S-CT cells at 0.1 C. The KB/S-CT cell has the highest initial discharge capacity of 1 419.6 mAh g^{-1} and the highest reversible capacity of 1 103.8 mAh g^{-1} after 50 cycles. However, the initial discharge capacities of the KB/S-T and KB/S cells are 1 318.7 and 1 081.4 mAh g^{-1}, and their retention capacities after 50 cycles are 1 016.8 and 805.6 mAh g^{-1}, respectively. Figs. 6b and c show the discharge capacity of the high plateau (Q_H: LiPS generation) and the low plateau (Q_L: Li_2S growth) of the KB/S, KB/S-T and KB/S-CT cells at 0.1 C. Due to the high conductivity and strong adsorption capacity of the CNT/$Ti_3C_2T_x$ aerogel, the KB/S-CT cell shows the highest Q_H value, indicating the sufficient conversion of S and the effective confinement of LiPSs. Moreover, the KB/S-CT cell also has the largest capacity in the low plateau (Q_L), which can be attributed to the low overpotential and accelerated redox conversion between liquid LiPSs and solid Li_2S. The excellent electrochemical performance at low current density proves that the CNT/$Ti_3C_2T_x$ aerogel modified separator can effectively immobilize LiPSs through the combined effect of high conductivity, electrochemical adsorption and catalytic ability. The rate performance of the KB/S, KB/S-T and KB/S-CT cells were further studied under continuously changing current density (Fig. 6d). At 0.1, 0.2, 1 and 2 C, the discharge capacities of the KB/S-CT cell are 1 446.4, 1 306.5, 1 117.5 and 1 043.2 mAh g^{-1}, re-

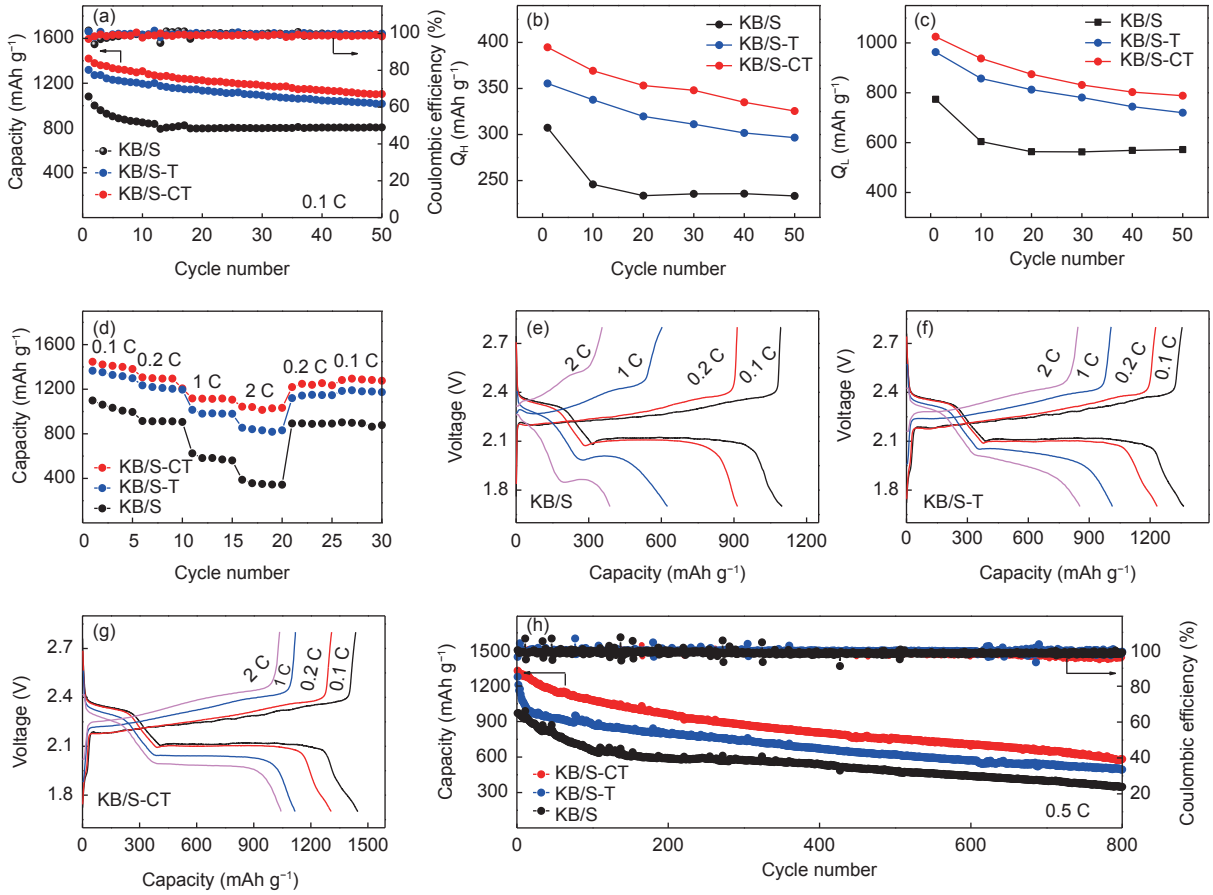

Fig. 6　(a) Cycling performance at 0.1 C. (b) High-plateau discharge capacities (Q_H) at 0.1 C. (c) Low-plateau discharge capacities (Q_L) at 0.1 C. (d) Rate performance. (e-g) Rate charge-discharge curves. (h) Cycling performance at 0.5 C.

spectively. When the current density suddenly returns to 0.2 C, a high rate capacity of 1 219.1 mAh g^{-1} can be recovered, demonstrating its remarkable rate ability, enhanced redox kinetics and superior structure robustness. Inversely, the discharge capacities of the KB/S-T and KB/S cells decrease rapidly as the current density increases. At 2 C, the capacities of the KB/S-T and KB/S cells are 854.3 and 387.6 mAh g^{-1}, respectively, which are much lower than that of the KB/S-CT cell. The rate charge-discharge curves of these cells are shown in Figs. 6e-g. The KB/S-CT cell can always maintain the complete and prolonged charge-discharge plateaus under all current densities, due to the fast reaction kinetics. Long-cycling performance was measured at 0.5 C to evaluate the practicality of the CNT/$Ti_3C_2T_x$ aerogel modified separator in Li–S batteries (Fig. 6h). The initial discharge capacities of the KB/S-CT, KB/S-T and KB/S cells are 1 329.7, 1 278.1 and 970.5 mAh g^{-1}, respectively. After 800 cycles, the KB/S-T and KB/S cells show a relatively poor cycling stability. While the KB/S-CT cell remains the highest reversible capacity of 582.8 mAh g^{-1}, and the average capacity fading rate per cycle is 0.07%, indicating its outstanding cycling stability.

The high discharge capacity and the long cycling life of the KB/S-CT cell can be attributed to the following unique structural superiorities of the CNT/$Ti_3C_2T_x$ aerogel modified separator. First, construction of the 3D interconnected aerogel structure effectively prevents the restacking of $Ti_3C_2T_x$ flakes, which not only offers effective channels for charge transfer, but also exposes abundant active sites that interact with LiPSs. Second, introduction of the CNTs helps to establish an open but robust conductive network at the cathode/separator interface, greatly improving the mechanical strength and the conductivity of the aerogel. As a result, enhanced LiPS adsorption,

fast ion/electron transport, and effective catalytic conversion can be achieved simultaneously, thereby restraining the shuttle effect and promoting the reaction kinetics.

4 Conclusions

A 3D porous CNT/$Ti_3C_2T_x$ aerogel composed of highly active $Ti_3C_2T_x$ and conductive CNTs networks was successfully synthesized, and used as a LiPS regulator to modify the commercial PP separator. This aerogel exhibits excellent conductivity for electron transfer, strong adsorption capacity for LiPSs and high catalytic activity for accelerated conversion kinetics. Based on the favorable anchoring-conversion mechanism, the Li–S cell assembled with the CNT/$Ti_3C_2T_x$ aerogel modified separator exhibits superior discharge capacity, long cycling life and outstanding rate performance, such as ultrahigh discharge capacity of 1 419.6 mAh g^{-1} at 0.1 C, low capacity fading rate per cycle of 0.07% after 800 cycles at 0.5 C as well as high rate capacity of 1 043.2 mAh g^{-1} even at 2 C. Our study can provide a novel idea for designing other 3D MXene composite materials used in Li–S batteries.

Acknowledgements

This work was supported by National Natural Science Foundation of China (52072099, 51772069).

References

[1] Chen X, Hou T Z, Persson K A, et al. Combining theory and experiment in lithium–sulfur batteries: Current progress and future perspectives[J]. Materials Today, 2019, 22: 142-158.

[2] Ren W C, Ma W, Zhang S F, et al. Recent advances in shuttle effect inhibition for lithium sulfur batteries[J]. Energy Storage Materials, 2019, 23: 707-732.

[3] Zeng S B, Li L G, Yu J P, et al. Highly crosslinked organosulfur copolymer nanosheets with abundant mesopores as cathode materials for efficient lithium–sulfur batteries[J]. Electrochimica Acta, 2018, 263(10): 53-59.

[4] Ren W C, Ma W, Zhang S F, et al. Nitrogen-doped carbon fiber foam enabled sulfur vapor deposited cathode for high performance lithium sulfur batteries[J]. Chemical Engineering Journal, 2018, 341(1): 441-449.

[5] Chen S R, Wang D W, Zhao Y M, et al. Superior performance of a lithium–sulfur battery enabled by a dimethyl trisulfide containing electrolyte[J]. Small Methods, 2018, 2(6): 1800038.

[6] Chen L, Fan L Z. Dendrite-free Li metal deposition in all-solid-state lithium sulfur batteries with polymer-in-salt polysiloxane electrolyte[J]. Energy Storage Materials, 2018, 15: 37-45.

[7] Li Q, Zeng F L, Guan Y P, et al. Poly (dimethylsiloxane) modified lithium anode for enhanced performance of lithium –sulfur batteries[J]. Energy Storage Materials, 2018, 13: 151-159.

[8] Zhao J, Zhou G M, Yan K, et al. Air-stable and freestanding lithium alloy/graphene foil as an alternative to lithium metal anodes[J]. Nature Nanotechnology, 2017, 12: 993-999.

[9] He Y B, Qiao Y, Zhou H S. Recent advances in functional modification of separators in lithium –sulfur batteries[J]. Dalton Transactions, 2018, 47(20): 6881-6887.

[10] Deng N P, Kang W M, Liu Y B, et al. A review on separators for lithium–sulfur battery: Progress and prospects[J]. Journal of Power Sources, 2016, 331(1): 132-155.

[11] Liao H Y, Zhang H Y, Hong H Q, et al. Novel flower-like hierarchical carbon sphere with multi-scale pores coated on PP separator for high-performance lithium-sulfur batteries[J]. Electrochimica Acta, 2017, 257: 210-216.

[12] Zheng B B, Yu L W, Yang Z, et al. Ultralight carbon flakes modified separator as an effective polysulfide barrier for lithium-sulfur batteries[J]. Electrochimica Acta, 2019, 295: 910-917.

[13] Zhu L, Jiang H T, Yang Q Y, et al. An effective porous activated carbon derived from puffed corn employed as the separator coating in a lithium-sulfur battery[J]. Energy Technology, 2019, 7(11): 1900752.

[14] Feng G L, Liu X H, Wu Z G, et al. Enhancing performance of Li-S batteries by coating separator with MnO@yeast-derived carbon spheres[J]. Journal of Alloys and Compounds, 2020, 817: 152723.

[15] Shao Z T, Wu L L, Yang Y, et al. Carbon nanotube-supported $MoSe_2$ nanoflakes as an interlayer for lithium-sulfur batteries[J]. New Carbon Materials, 2021, 36(1): 219-226.

[16] Li H P, Sun L C, Zhao Y, et al. A novel CuS/graphene-coated separator for suppressing the shuttle effect of lithium/sulfur batteries[J]. Applied Surface Science, 2019, 466(1): 309-319.

[17] Fan Y P, Niu Z H, Zhang F, et al. Suppressing the shuttle effect in lithium –sulfur batteries by a UiO-66-modified polypropylene separator[J]. ACS Omega, 2019, 4(6): 10328-10335.

[18] Jin Q, Li L, Wang H R, et al. Dual effects of the carbon fibers/$Ti_3C_2T_x$ interlayer on retarding shuttle of polysulfides for stable lithium –sulfur batteries[J]. Electrochimica Acta, 2019, 312(20): 149-156.

[19] Jin Q, Zhang N, Zhu C C, et al. Rationally designing S/$Ti_3C_2T_x$ as a cathode material with an interlayer for high-rate and long-cycle lithium-sulfur batteries[J]. Nanoscale, 2018, 10(35): 16935-16942.

[20] Liang X, Rangom Y, Kwork C Y, et al. Interwoven MXene nanosheet/carbon-nanotube composites as Li-S cathode hosts[J]. Advanced Materials, 2017, 29(3): 1603040.

[21] Bao W Z, Liu L, Wang C Y, et al. Facile synthesis of crumpled

nitrogen-doped MXene nanosheets as a new sulfur host for lithium-sulfur batteries[J]. Advanced Energy Materials, 2018, 8(13): 1702485.

[22] Li J, Jin Q, Yin F, et al. Effect of $Ti_3C_2T_x$-PEDOT: PSS modified-separators on the electrochemical performance of Li-S batteries[J]. RSC Advances, 2020, 10: 40276.

[23] Yin F, Jin Q, Gao H, et al. A strategy to achieve high loading and high energy density Li-S batteries[J]. Journal of Energy Chemistry, 2021, 53: 340-346.

[24] Liang X, Garsuch A, Nazar L F. Sulfur cathodes based on conductive MXene nanosheets for high performance lithium-sulfur batteries[J]. Angewandte Chemie International Edition, 2015, 127(13): 3907-3911.

[25] Wang X Y, Fu Q S, Wen J, et al. 3D $Ti_3C_2T_x$ aerogels with enhanced surface area for high performance supercapacitors[J]. Nanoscale, 2018, 10: 20828-20835.

[26] Song J J, Guo X, Zhang J Q, et al. Rational design of free-standing 3D porous MXene/rGO hybrid aerogels as polysulfide reservoirs for high-energy lithium-sulfur batteries[J]. Journal of Materials Chemistry A, 2019, 7(11): 6507-6513.

[27] Meng Q H, Jin Q, Wang H R, et al. 3D $Ti_3C_2T_x$ aerogel-modified separators for high-performance Li –S batteries[J]. Journal of Alloys and Compounds, 2020, 816: 153155.

[28] Sambyal P, Iqbal A, Hong J, et al. Ultralight and mechanically robust $Ti_3C_2T_x$ hybrid aerogel reinforced by carbon nanotubes for electromagnetic interference shielding[J]. ACS Applied Materials & Interfaces, 2019, 11(41): 38046-38054.

[29] Ding X H, Li C H, Li Y C. Thermal stability and photocatalysis of a novel two-dimensional MXene[J]. Hans Journal of Chemical Engineering and Technology, 2018, 8(5): 326-332.

[30] Cheng Y Y, Huang J F, Qi H, et al. Adjusting the chemical bonding of SnO_2@CNT composite for enhanced conversion reaction kinetics[J]. Small, 2017, 13(31): 1700656.

[31] Wang R X, Wang K L, Gao S, et al. Rational design of yolk-shell silicon dioxide@hollow carbon spheres as advanced Li-S cathode hosts[J]. Nanoscale, 2017, 9(39): 14881-14887.